Self-adhesive electrode applied to ZnO nanorod-based piezoelectric nanogenerators

Self-adhesive electrode applied to ZnO nanorod-based piezoelectric nanogenerators

Pelin Yilmaz[1], Peter Greenwood[2], Simone Meroni[2], Joel Troughton[2], Petr Novák [3], Xuan Li,[1] Trystan Watson[2], and Joe Briscoe[1*]

[1]School of Engineering and Materials Science, Queen Mary University of London, Mile End Road, London E1 4NS, United Kingdom

[2] SPECIFIC, College of Engineering, Swansea University, Bay Campus, Swansea, SA1 8EN, United Kingdom

[3] New Technologies – Research Centre, University of West Bohemia, Czech Republic

*e-mail: j.briscoe@qmul.ac.uk

Abstract

ZnO nanorod-based piezoelectric devices have gained wide attention in energy harvesting systems as they can be processed at low temperatures onto flexible plastic substrates, giving a good potential for low cost. However, the vacuum-evaporated, precious metal contacts remain a high-cost element of the devices. This paper discusses the use of transparent conductive adhesives (TCAs) as an alternative top contact that is free from both vacuum-evaporation and precious metals. TCA films of various thicknesses were tape-cast onto nickel microgrid on PET substrates and adhered using low-pressure cold-lamination to bond the adhesive component of the TCA to piezoelectric generators with the final device structure of PET/ITO/ZnO-seed/ZnO-nanorods/CuSCN/PEDOT:PSS/TCA. The piezoelectric performances of the devices were compared by measuring output voltage in open-circuit and maximum power output across a range of resistive loads. The voltage output was observed to rise with increasing TCA thickness, reaching a maximum value of 0.72 V generated with 110 µm of TCA as top contact. However, the higher resistance due to increased TCA thickness led to decreased power output; a maximum calculated power of 0.25 µW was obtained from the device with the thinnest TCA layer of 22 µm. Finally, the performance of piezoelectric nanogenerators with TCA contacts were compared to a control device with an evaporated gold contact.

1. Introduction

Piezoelectric energy harvesters have been of interest for some time as one of a class of vibration/kinetic energy harvesters that includes electrostatic and electromagnetic energy harvesters [1,2]. These have a wide range of potential applications where localised, generally low-level power can be harvested from the environment to power portable devices and sensors, removing or reducing the need for batteries or complex and expensive wiring. In particular, the growth in interest in the Internet of Things has driven a renewed interest in energy harvesting, as the proposed network of

miniaturised and distributed sensors would be most effective if removed from the dependency on batteries and their necessary replacement.

For more than ten years there has been widespread development of ZnO nanorods for piezoelectric energy harvesting (nanogenerators) due to their low-cost and simple, solution-based fabrication. This enables the coating of a wide range of substrates, including polymers, in nanorod arrays that can be used for energy harvesting [3], offering the potential for low-cost and adaptable energy harvester fabrication. In our previous work, we have demonstrated an alternative ZnO nanogenerator, which uses a semiconducting polymer poly(3,4-ethylenedioxythiophene) poly(styrenesulfonate) (PEDOT:PSS) to coat the surface of the ZnO nanorods [4], producing a lower impedance and higher output power than alternative designs with insulating polymer coatings [5]. We have also shown that a surface passivating layer of the semiconductor CuSCN produces large increases in output power [6]. However, a serious hindrance remains to the low-cost, mass fabrication of these devices: the need for a vacuum-evaporated gold top contact. Such evaporated (or sputtered), precious metal contacts are also found in many other nanostructured energy harvesting devices [7–14] and therefore a viable, low-cost alternative would be extremely attractive for the energy harvesting, and wider community.

Here we report the innovative use of transparent conductive adhesives (TCAs) as top electrodes instead of conventional gold contacts. TCAs can be good alternatives to replace gold by omitting the vacuum deposition step and precious metal content of gold evaporation. These TCAs have been demonstrated to work as effective top contacts for hybrid organic-inorganic lead halide perovskite photovoltaics [15,16] and electroluminescent devices [17], but have never been demonstrated in a kinetic energy harvester. The PEDOT:PSS layer in our devices – to which the TCA has been shown to adhere well and form a good electrical contact [15,16] – offers a good opportunity to demonstrate this alternative contact material. The influence of TCA contacts was investigated for devices with TCA thickness ranging from 22 to 134 µm. The devices were characterised by DC current-voltage measurements, AC impedance spectroscopy (IS), and open-circuit voltage output of the devices was measured by bending them to 45° and releasing. Maximum power output across a range of loads was also assessed by oscillating the devices on a permanent magnetic shaker. Functioning nanogenerators with varied TCA contact thickness were successfully produced where a voltage output was obtained responding to a strain change. The results were compared to study the optimum thickness of the TCA layers and how the thickness impacts on the overall properties and performance of the nanogenerator devices. The piezoelectric performances of TCA devices were also compared with a control device which has the same device structure but with a gold layer as top contact. Our study has shown that thicker TCA films generate higher open circuit voltage but lower power output due to the increased device resistance with greater TCA thickness. Open-circuit voltage over 0.5 V was obtained from devices with 110 and 134 µm thick TCA layers. A TCA thickness of 22 µm gave a maximum power output of 0.25 µW. These results were lower compared to the control device with open circuit voltage output of ~0.7 V and maximum power of 4.67 µW. However, TCA devices still hold a good promise for a potential use in nanogenerator applications thanks to their low cost and easier processing methods.

2. Experimental Methods

2.1. Fabrication of Piezoelectric Devices

The piezoelectric device was fabricated by synthesizing layers of the following structure: PET/ITO/ZnO seeds/ZnO nanorods/CuSCN/PEDOT:PSS/TCA. ZnO nanorods were grown using an aqueous solution method on 2 x 1 cm^2 PET/ITO (polyethylene/indium-tin oxide) substrates (Sigma Aldrich, surface resistivity 60 Ω/□). These had previously been coated with a 100 nm-thick ZnO seed layer by magnetron sputtering [18]. An equimolar precursor solution of 25 mM $Zn(NO_3)_2$ (Alfa Aesar, 99%) and

25 mM hexamethylenetetramine (HMT) (Alfa Aesar, 99%) in deionised water was used for ZnO nanorod synthesis. The synthesis was carried out for 24 hours at 90°C without any further treatment. ZnO nanorods were then spray coated with a thin layer of 0.15 M CuSCN (Aldrich, 99%) solution in dipropyl sulphide (Alfa Aesar, 98+%) by using a spray gun. An optimised amount of 8 ml of CuSCN solution was sprayed per three substrates, which were mounted on a hotplate at 100°C to evaporate the dipropyl sulphide. A further layer of poly(3,4-ethylenedioxythiophene) poly(styrenesulfonate) (PEDOT:PSS, Aldrich, 1.3 wt% in water, conductive grade) was deposited on CuSCN-coated ZnO nanorods by similar spray coating method. The insulating polyurethane (PU) resin was coated on the left side of the device before attaching the top contacts to avoid short circuit between the opposite contacts. The "transparent conductive adhesive" (TCA) top contacts were prepared by tape casting the PEDOT:PSS-acrylic adhesive blend onto the transparent conductive film (nickel microgrid on PET: Epigem, Epimesh) in accordance with established methods [15]. The height of the tape-casting guide was varied, using between 2 and 10 layers of adhesive tape to produce TCA films with a dry thickness ranging from 22 to 134 µm. The PET/nickel microgrid/TCA Top contacts were adhered to the devices using low-pressure cold lamination to bond the adhesive component with the PEDOT:PSS surface of the nanogenerator. Devices were completed by bonding copper strips to each contact using silver epoxy with final encapsulation using PET laminating pouches to seal the whole device **(Figure 1)**. Three devices were fabricated for each TCA thickness.

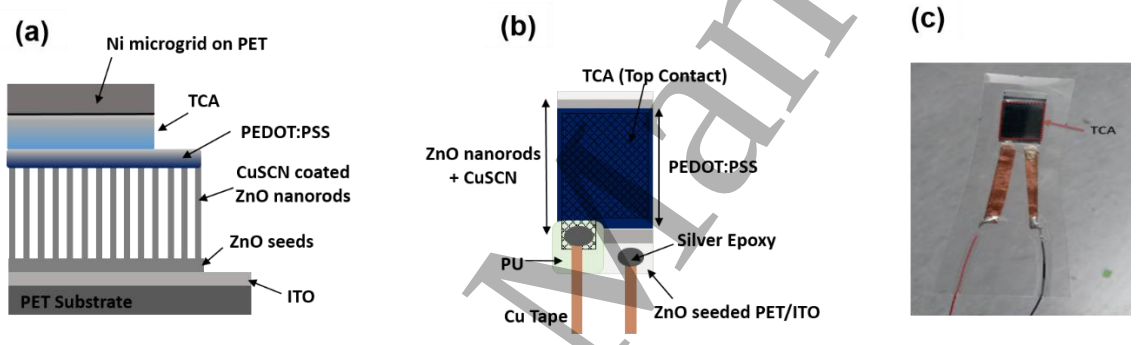

Figure 1. (a) Cross section and (b) top view schematics of the device. (c) Complete nanogenerator device.

2.2. Testing of Devices

Impedance spectroscopy (IS) was conducted using a Gamry Interface 1000 Potentiostat. The input frequency range used was from 0.1 Hz to 1 MHz. Open-circuit voltages were measured with an oscilloscope (Tektronix TDS 2012C) by manually bending the devices to 45° and releasing. For assessment of power outputs, the devices were mounted on a thin 1 cm x 4 cm spring-steel cantilever which was fixed on a permanent magnetic shaker (Brüel & Kjær, LDS V406) (Schematics in Supporting Information **Figure S1**). The root-mean-square (RMS) voltage outputs were measured across a range of resistive loads introduced by resistance box connected to the devices when the device/cantilever was oscillating at its resonant frequency (~300 Hz) with a peak acceleration of 12.4g. RMS power outputs were correspondingly calculated from the following equation:

$$Power\ (W) = \frac{(Voltage\ Output\ (V))^2}{Resistive\ Load\ (\Omega)} \qquad (1)$$

3. Results and Discussion

3.1. Device Structure

The morphology and dimensions of each layer of the device structure were analysed using scanning electron microscopy (SEM). The aqueous solution synthesis method at low temperature of 90°C

provided a uniform and densely packed array of ZnO nanorods growth on PET substrates **(Figure 2a-b)**. The nanorods were approximately 4 µm in length and 80 nm in diameter on average. CuSCN coating can just be seen as a thin layer on the surface of the nanorods, in some cases filling between rods which are close together **(Figure 2c)**. The CuSCN coverage was ~5-10 nm thick, however was not completely uniform **(Figure 2c)**. A layer of PEDOT:PSS was spray-coated onto the nanorod surface to provide a capping layer to allow addition of a top contact. The PEDOT:PSS layer was found to be ~2 µm thick by SEM analysis of material removed from the device surface **(Figure S2)**. In order to analyse the full device structure, complete devices were cryogenically fractured and analysed by SEM (**Figure 2d**). The ZnO nanorod array can be seen embedded in the thick PEDOT:PSS/TCA layer. No interface could be found between the spray-coated PEDOT:PSS layer and the TCA layer, indicating excellent adhesion. The thickness of the TCA layer for this device (cast using 6 tape layers) was measured to be 82 µm, in excellent agreement with the profilometer measurement (see below). Overall, this analysis demonstrates the excellent adhesion of the TCA to the PEDOT:PSS surface, and in turn the PEDOT:PSS to the ZnO nanorods.

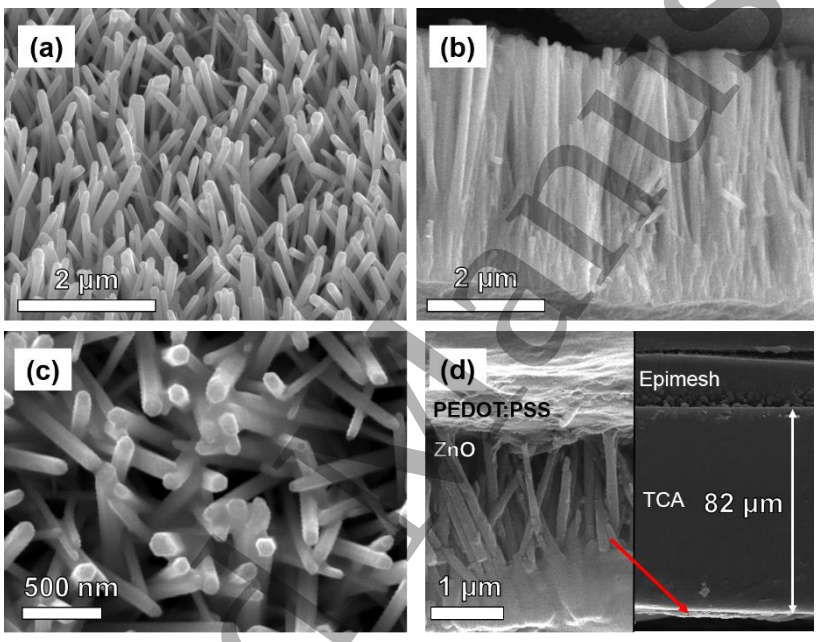

Figure 2. (a) Tilted and (b) cross section SEM image of ZnO nanorods grown on ITO-coated PET substrates. (c) Tilted SEM image of CuSCN coated ZnO nanorods. (d) Cross section SEM images of full device showing close-up of ZnO nanorods embedded in PEDOT:PSS layer (left), and cross-section of full, 82 µm TCA film on nickel microgrid/PET with ZnO layer at bottom. Thickness of TCA layer indicated, with Ni microgrid layer and edge of PET layer visible above.

The thickness of the TCA films was measured using a stylus profilometer (Dektak, D150); predictably, an approximately linear trend between film thickness and casting height was found **(Figure 3)**. The mean TCA thickness were 22, 46, 82, 110, and 134 µm for nominal casting heights of 2, 4, 6, 8, and 10 tape layers. The overlaid profilometer scans **(Figure 3b)** show the region at the edge of each film used for the thickness measurement. The standard error of the mean for each sample is indicated by the shaded region; this error generally increases with the number of tape layers used to form the casting guide. The variation in film thickness is typical of the inconsistency exhibited by the tape casting process and can be eliminated with a scalable coating technique such as doctor blading or screen-printing.

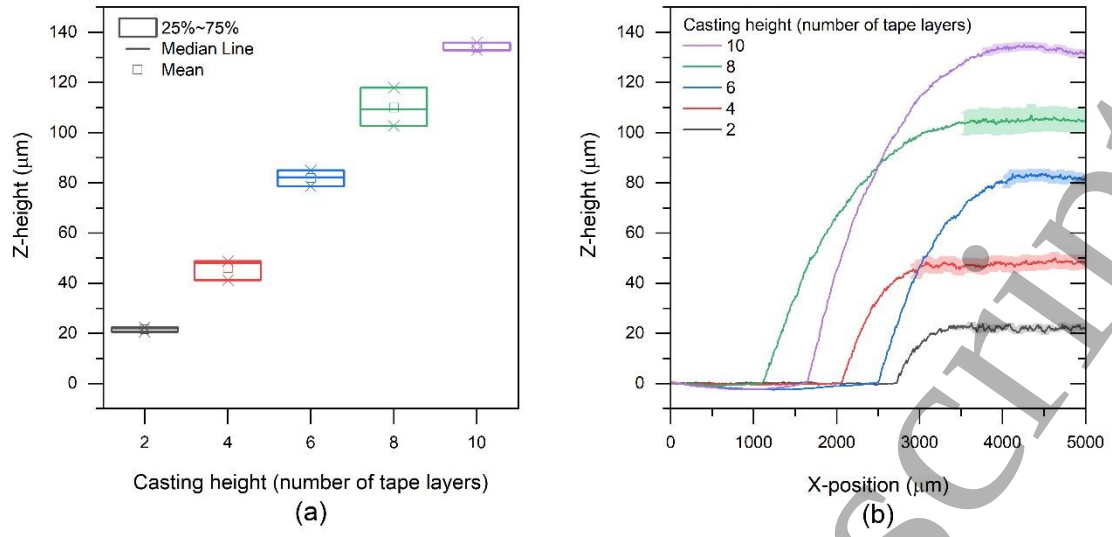

Figure 3. (a) Summary of the TCA thickness data. (b) Topography of TCA film-edge used for the thickness measurement, the shading represents the standard error of the mean thickness.

3.2. Electrical Impedance Characteristics

Impedance spectroscopy (IS) measurements were performed to understand the charge transfer kinetics occurring at the interfaces of the layered structures. The impedance spectra generally appear to comprise three semi-circular elements **(Figure 4)**. More information, including the nature of these elements, and their capacitance, can be obtained by fitting an equivalent circuit to the data. Due to the presence of three semicircles, it is assumed that the equivalent circuit comprises of three RC elements in series, with additional series resistance (**Figure 4 inset)**. These would logically correspond to: 1. the main device structure of ZnO/CuSCN/PEDOT:PSS, which generally gives a single semicircle in a Nyquist plot [5]; 2. The PEDOT:PSS/TCA interface; 3. The TCA layer itself. A fit was therefore performed on these impedance data using this equivalent circuit. The full fit is shown in the supporting information (**Figure S3**), which gave the parameters shown in **Table 1.** The high capacitance of the *RC* element R_2-C_2 suggests that this may correspond to the TCA film, which would be expected to have high capacitance. However, further control experiments of various combinations of each element would be needed to confirm this for certain.

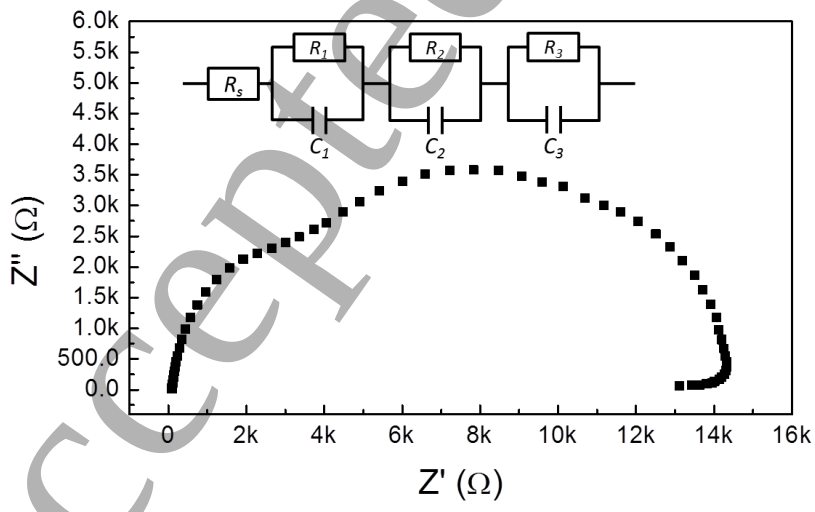

Figure 4. Example Nyquist plot for 6-layer device. Suggested equivalent circuit is shown in inset.

Table 1. Parameters obtained from fitting equivalent circuit model to impedance data shown in **Figure 4**.

Element	Resistance, kΩ	Capacitance, μF)
R_s	0.16 ± 0.03	
R_1, C_1	3.69 ± 0.10	0.114 ± 0.004
R_2, C_2	4.34 ± 0.14	10.9 ± 0.8
R_3, C_3	5.92 ± 0.13	0.92 ± 0.04

Total device resistance was assessed from the maximum real component of the complex impedance. When plotted against the thickness of the TCA layer a weak trend was observed between device resistance and thickness, with a large error for the resistance of each layer **(Figure 5)**. This seems to suggest that there is a slight increase in the device resistance as the TCA thickness increases. This is to be expected as the TCA is a relatively poor conductor when compared to the ITO electrode and nickel microgrid on PET materials between which the device is formed (60 Ω/□ and 1.2 Ω/□ respectively). The linear trend has a slope of 11.8 Ω/μm, with an intercept of 13.9 kΩ. This suggests an increase of 11.8 Ω per μm of TCA (bulk TCA film resistance), with a basic device resistance of 13.9 kΩ. This basic resistance would correspond to the resistance of the ITO/ZnO/CuSCN/PEDOT:PSS structure, as well as the PEDOT:PSS/TCA interface and nickel microgrid resistances. This agrees well with a device resistance measured for our previous devices of ~12 kΩ [5], with the additional 1.9 kΩ originating from the PEDOT:PSS/TCA interface and nickel microgrid on PET substrate. Also, comparing the estimate of 11.8 Ω per μm to *RC* element 2 from the fit above (**Table 1**) – which gave a resistance of 4.34 kΩ for a 6-layer (82 μm) device – gives ~53 Ω per μm. This is within a factor of 5 of that obtained from the slope in **Figure 5**, which, considering the large error in the data points, suggests that a TCA resistance per thickness in this range is reasonable. The large error originates from large device-to-device variability, most likely from the quality of the bond to the TCA layer. Reduction of this variability is the subject of ongoing work.

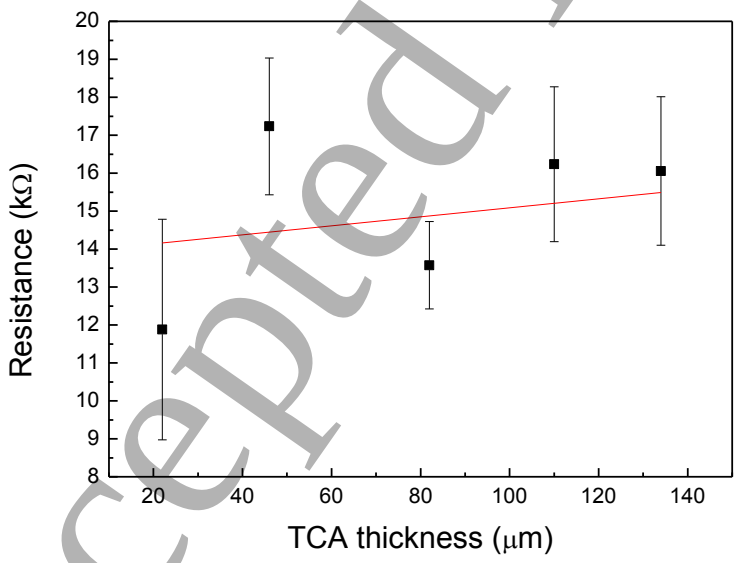

Figure 5. Average resistance values for the nanogenerator devices depending on TCA layer thickness.

3.3. Device Output

It can be seen from **Figure 6** that functioning nanogenerators with TCA top contacts were successfully produced where an output voltage was obtained upon applying strain (45° bend and manual release); this example device with a 46 µm TCA layer produced a peak open circuit voltage around ~0.4 V. Full device performance testing was conducted by measuring maximum open-circuit output voltage from such traces, and average (RMS) power output across a range of resistive loads when vibrated using a mechanical shaker (see methods).

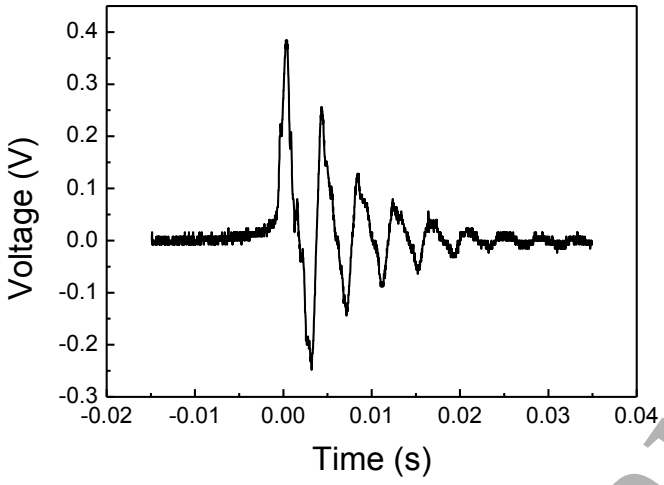

Figure 6. Open circuit voltage output of a nanogenerator device with a 46 µm thick TCA layer when bent and released manually.

Figure 7 shows the peak open-circuit voltage output of all nanogenerator devices plotted against the TCA layer thickness with each data point representing the average of three devices. The measured voltage output was higher for nanogenerators with a thicker TCA layer: the 110 and 134 µm devices gave an average value of more than 0.5 V. This could be expected due to the increasing resistance of the device with increased TCA thickness, as calculated by the IS measurements; we have shown in our previous work that these devices are strongly affected by polarisation screening from the circuit, and that this can be slowed by increasing the *RC* time constant ($\tau = RC$), giving higher voltage outputs with higher internal resistance [6]. Hence the need for electrical impedance matching to maximise power transfer [19,20], as investigated below.

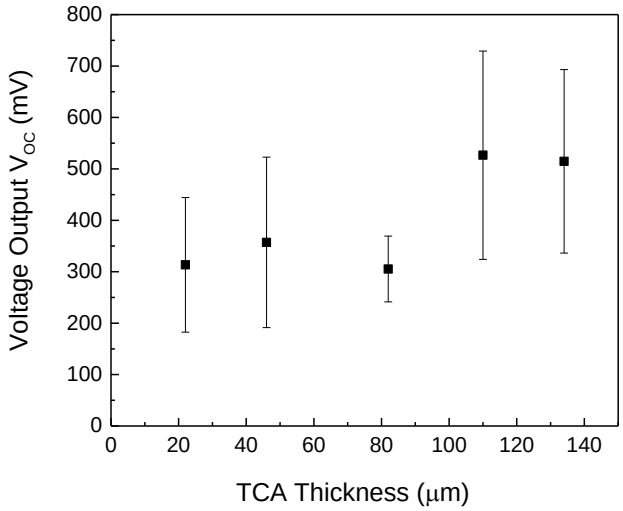

Figure 7. Peak open circuit voltage output of all devices with different thicknesses of TCA layers.

To more accurately assess the useful output from the devices, RMS voltage output was measured across a range of resistive loads. Correspondingly, RMS power output obtained by the devices at different resistive loads were calculated. These measurements were conducted when the devices were mounted on an oscillating cantilever fixed on a magnetic shaker at an acceleration of 12.4g. The RMS voltage output was then measured from the sinusoidal oscillation of the cantilever at resonant frequency (~300 Hz). An example plot of power versus resistive load for a device with a 22 μm TCA layer is shown in **Figure 8** (See Figure S4 for plots of all devices).

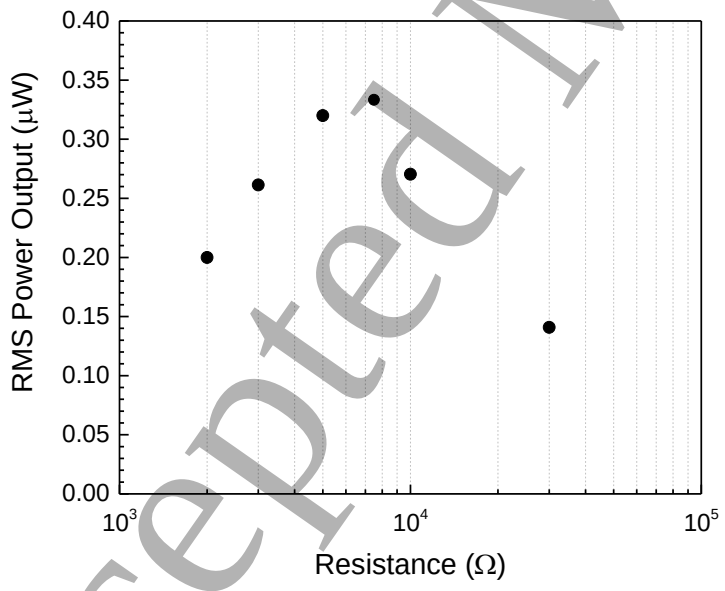

Figure 8. RMS power output calculated by measuring RMS voltage outputs across a range of resistive loads for an example 22 μm TCA layer device. Maximum power was obtained at a resistance load of 7500 Ω.

Using this method, the maximum RMS output power and optimum load were obtained for all nanogenerator devices. The average of this maximum power versus TCA layer is reported in **Figure 9,**

which was calculated by taking an average of the maximum powers obtained by the devices of same TCA thickness. The highest power output was obtained devices with a 22 μm TCA layer reaching an average value of 0.25 μW. The power output decreases with increasing TCA thickness. This is related to the higher internal (series) resistance of devices with a thicker TCA component causing a reduction in power output. This suggests a thin TCA film is desirable to reduce resistive losses for an increased power output despite the increased open-circuit voltage with increasing TCA thickness. We previously demonstrated that open-circuit voltage is a somewhat misleading measure of device performance, as it will generally increase with increasing internal resistance (due to the principle of a resistive divider), but power output will decrease where this resistance is added externally to the piezoelectric element [5].

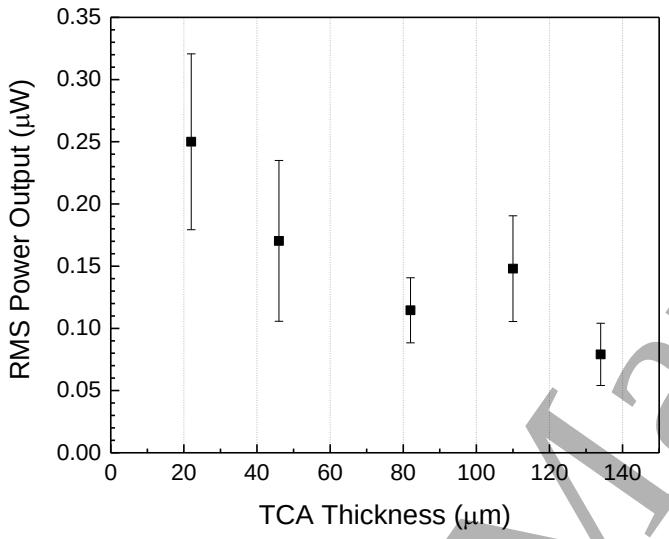

Figure 9. Maximum RMS power obtained at different TCA layer thickness. The power increases with decreasing TCA thickness, where the average power for nanogenerator devices with a 22 μm thick TCA layer was the highest at 0.25 μW.

The output open-circuit voltage and RMS power output on a range of loads of a control device were also measured for comparison **(Figure S5)**. The control device had an identical basic device structure as the TCA-containing devices (PET/ITO/ZnO seeds/ZnO nanorods/CuSCN/PEDOT:PSS) but with ~150 nm of evaporated gold as top contact. The peak open-circuit voltage of the control device was found to be higher than all the TCA devices, reaching an average value of ~686 mV **(Table 2)**. Although the internal resistance of this device was lower than the TCA devices, the losses are also expected to be lower, accounting for the higher output. In addition, the mechanical resonance of the device clearly has a longer duration (Figure S5b). This is related to the different mechanical properties of the device, as the TCA-containing devices are mechanically stiffer due to the nickel microgrid on PET films on which TCA layer is deposited. To demonstrate, a simple stiffness test was conducted to calculate and compare the flexural constants (k) of the devices (which is proportional to the modulus of elasticity) by measuring the maximum displacement upon applying the equal force. It was found that a 2 layer TCA containing device has a higher flexural constant, with ratio of k_{TCA}/k_{Gold} = 1.43 compared to the device with gold contact, which implies less flexibility and explains the stronger damping of oscillation with TCA devices (See Figure S6 for experimental details and detailed calculations). To alleviate this in future a more compliant conductive substrate could be used as a basis for the TCA layer since in this application the transparency of the Ni microgrid is not needed, unlike the photovoltaic applications for which is was developed [15,16].

Table 2. Piezoelectric performance parameters for all TCA devices with different thickness of TCA layers and control device with Au layer as top contact

Contact	Open Circuit Voltage, mV	Peak Power, µW)
TCA - 22 µm	69 ± 32	0.3 ± 0.1
TCA - 46 µm	360 ± 170	0.2 ± 0.1
TCA - 82 µm	305 ± 64	0.1 ± 0.03
TCA - 110 µm	530 ± 200	0.15 ± 0.04
TCA - 134 µm	520 ± 180	0.08 ± 0.03
Au	690 ± 210	4.7 ± 2.6

4. Conclusions

The use of transparent conductive adhesives (TCAs) as top-contact electrodes in piezoelectric devices has been demonstrated for the first time. The top-contacts were prepared by tape-casting the TCA at different thicknesses on nickel microgrid on PET substrates and applied to the devices using low-pressure cold-lamination. The piezoelectric performance of the devices was evaluated by measuring output voltage in open-circuit and maximum power output across a range of resistive loads. It was found that the peak voltage output increased for thicker TCA layers, where a maximum voltage output of 0.72 V was generated when a device with 110 µm of TCA was bent and released manually. However, higher internal resistance introduced by increasing TCA thickness led to a reduced power output; a maximum calculated power of 0.25 µW was obtained from the device 22 µm of TCA. Devices with TCA contacts were also compared to a control device, where the top contact was ~150 nm of evaporated gold. The control device generated a higher power reaching an average value of 4.67 µW. This was expected due to the lower resistance of the gold layer and higher strain induced due to its less stiff structure. However, the piezoelectric performances of TCA devices are still within one order of magnitude of the control device, therefore, they have good promise for replacing the expensive and difficult-to-produce gold contacts. These results suggest that further lowering of the TCA resistance, for example by increasing the PEDOT:PSS content, may improve nanogenerator output power further. This is possible for this application, where transparency is not needed, unlike previous applications of the TCAs in optoelectronic devices. Furthermore, this utilisation of the TCA contacts beyond the initial demonstrations in optoelectronic devices indicate there may be many more applications to which these contacts could be applied to facilitate low-cost and high-throughput device manufacture.

5. Acknowledgements

JB acknowledges support from Innovate UK project number 101796. PN acknowledge support from CENTEM projects CZ.1.05/2.1.00/03.0088 and PLUS LO1402 (Czech Republic).

References

[1] Beeby S P, Tudor M J and White N M 2006 Energy harvesting vibration sources for microsystems applications *Meas. Sci. Technol.* **17** R175

[2] Cook-Chennault K A, Thambi N and Sastry A M 2008 Powering MEMS portable devices—a review of non-regenerative and regenerative power supply systems with special emphasis on

piezoelectric energy harvesting systems *Smart Mater. Struct.* **17** 043001

[3] Briscoe J and Dunn S 2014 Piezoelectric nanogenerators - a review of nanostructured piezoelectric energy harvesters *Nano Energy* **14** 15–29

[4] Briscoe J, Stewart M, Vopson M, Cain M, Weaver P M and Dunn S 2012 Nanostructured p-n junctions for kinetic-to-electrical energy conversion *Adv. Energy Mater.* **2** 1261–8

[5] Briscoe J, Jalali N, Woolliams P, Stewart M, Weaver P M, Cain M and Dunn S 2013 Measurement techniques for piezoelectric nanogenerators *Energy Environ. Sci.* **6** 3035–45

[6] Jalali N, Woolliams P, Stewart M, Weaver P M, Cain M G, Dunn S and Briscoe J 2014 Improved performance of p–n junction-based ZnO nanogenerators through CuSCN-passivation of ZnO nanorods *J. Mater. Chem. A* **2** 10945

[7] Saravanakumar B, Mohan R, Thiyagarajan K and Kim S-J 2013 Fabrication of a ZnO nanogenerator for eco-friendly biomechanical energy harvesting *RSC Adv.* **3** 16646

[8] Lee S, Lee J, Ko W, Cha S, Sohn J, Kim J, Park J, Park Y and Hong J 2013 Solution-processed Ag-doped ZnO nanowires grown on flexible polyester for nanogenerator applications. *Nanoscale* **5** 9609–14

[9] Kim K-H, Kumar B, Lee K Y, Park H-K, Lee J-H, Lee H H, Jun H, Lee D and Kim S-W 2013 Piezoelectric two-dimensional nanosheets/anionic layer heterojunction for efficient direct current power generation. *Sci. Rep.* **3** 2017

[10] van den Heever T S and Perold W J 2013 Comparing three different energy harvesting circuits for a ZnO nanowire based nanogenerator *Smart Mater. Struct.* **22** 105029

[11] Lee M, Chen C Y, Wang S, Cha S N, Park Y J, Kim J M, Chou L J and Wang Z L 2012 A hybrid piezoelectric structure for wearable nanogenerators *Adv. Mater.* **24** 1759–64

[12] Hu Y, Lin L, Zhang Y and Wang Z L 2012 Replacing a Battery by a Nanogenerator with 20 V Output *Adv. Mater.* **24** 110–4

[13] Kang P G, Yun B K, Sung K D, Lee T K, Lee M, Lee N, Oh S H, Jo W, Seog H J, Ahn C W, Kim I W and Jung J H 2014 Piezoelectric power generation of vertically aligned lead-free (K,Na)NbO_3 nanorod arrays *RSC Adv.* **4** 29799

[14] Hwang G T, Park H, Lee J H, Oh S, Park K Il, Byun M, Park H, Ahn G, Jeong C K, No K, Kwon H, Lee S G, Joung B and Lee K J 2014 Self-powered cardiac pacemaker enabled by flexible single crystalline PMN-PT piezoelectric energy harvester *Adv. Mater.* **26** 4880–7

[15] Bryant, D., Greenwood, P., Troughton, J., Wijdekop, M., Carnie, M., Davies, M., Wojciechowski, K., Snaith, H., Watson T., Worsley D 2014 A Transparent Conductive Adhesive Laminate Electrode for High Efficiency Organic-Inorganic Lead Halide Perovskite Solar Cells *Adv. Mater.* 7499–504

[16] Troughton J, Bryant D, Wojciechowski K, Carnie M J, Snaith H, Worsley D A and Watson T M 2015 Highly efficient, flexible, indium-free perovskite solar cells employing metallic substrates *J. Mater. Chem. A* **3** 9141–5

[17] Bryant D, Greenwood P, Troughton J, Watson T, Jewell E and Worsley D 2014 Increased performance of printed electroluminescent devices using a transparent conductive laminate *J. Print Media Technol. Res.* **3** 253–60

[18] Novák P, Briscoe J, Kozák T, Kormunda M, Netrvalová M and Bachratá Š 2017 Optimization of sputtered ZnO transparent conductive seed layer for flexible ZnO-nanorod-based devices *Thin*

Solid Films

[19] Kim H, Priya S, Stephanou H and Uchino K 2007 Consideration of Impedance Matching Techniques for Efficient Piezoelectric Energy Harvesting *IEEE Trans. Ultrason. Ferroelectr. Freq. Control* **54** 1851–9

[20] Jabbar H, Jung H J, Chen N, Cho D H and Sung T H 2017 Piezoelectric energy harvester impedance matching using a piezoelectric transformer *Sensors Actuators A Phys.* **264** 141–50